BRL-TR-3133

DTIC FILE COPY

2

TECHNICAL REPORT BRL-TR-3133

BRL

AD-A226 390

EXPLOSIVE CONSOLIDATION OF COMBUSTION SYNTHESIZED TiB_2 AND TiC: MICROSTRUCTURAL PROPERTIES

L.J. KECSKES
T. KOTTKE
P.H. NETHERWOOD, JR.
R.F. BENCK
A. NIILER

AUGUST 1990

U.S. ARMY LABORATORY COMMAND

BALLISTIC RESEARCH LABORATORY
ABERDEEN PROVING GROUND, MARYLAND

90 09 12 024

NOTICES

UNCLASSIFIED

REPORT DOCUMENTATION PAGE

Form Approved
OMB No. 0704-0188

1. AGENCY USE ONLY *(Leave blank)*

2. REPORT DATE
August 1990

3. REPORT TYPE AND DATES COVERED
Final 1 Oct 87 - 1 Oct 89

4. TITLE AND SUBTITLE
Explosive Consolidation of Combustion Synthesized TiB_2 and TiC: Microstructural Properties

5. FUNDING NUMBERS
1L161102AH43
WU 61102A

6. AUTHOR(S)
L. J. Kecskes, T. Kottke, P. H. Netherwood Jr., R. F. Benck and A. Niiler

7. PERFORMING ORGANIZATION NAME(S) AND ADDRESS(ES)

8. PERFORMING ORGANIZATION REPORT NUMBER

9. SPONSORING/MONITORING AGENCY NAME(S) AND ADDRESS(ES)
U.S. Army Ballistic Research Laboratory
ATTN: SLCBR-DD-T
Aberdeen Proving Ground, MD 21005-5066

10. SPONSORING/MONITORING AGENCY REPORT NUMBER
BRL-TR-3133

11. SUPPLEMENTARY NOTES

12a. DISTRIBUTION/AVAILABILITY STATEMENT
Approved for public release; distribution unlimited

12b. DISTRIBUTION CODE

13. ABSTRACT *(Maximum 200 words)*

Near full density TiB_2, TiC, and $TiC-TiB_2$ composites have been fabricated by combustion synthesis reactions followed by dynamic consolidation of the still hot, porous, ceramic body. The relationship between the morphologies and purity of the precursor powders used and the ceramic product structures is presented. Intergrain bonding and residual porosity of the dynamically consolidated products are found to depend strongly on the impurity levels of the precursor powders. Analysis of the TiC indicates that the density and microhardness increase as a function of the C/Ti ratio with maximum values at the ratio of 1.0. Keywords:

14. SUBJECT TERMS
SHS, Combustion Synthesis, Explosive Compaction, Microstructure, Ceramics, Titanium Boride, Titanium Carbide. (JS)

15. NUMBER OF PAGES
41

16. PRICE CODE

17. SECURITY CLASSIFICATION OF REPORT	18. SECURITY CLASSIFICATION OF THIS PAGE	19. SECURITY CLASSIFICATION OF ABSTRACT	20. LIMITATION OF ABSTRACT
UNCLASSIFIED	UNCLASSIFIED	UNCLASSIFIED	UL

NSN 7540-01-280-5500

UNCLASSIFIED

Standard Form 298 (Rev. 2-89)
Prescribed by ANSI Std. Z39-18
298-102

INTENTIONALLY LEFT BLANK.

TABLE OF CONTENTS

INTENTIONALLY LEFT BLANK.

LIST OF FIGURES

LIST OF TABLES

ACKNOWLEDGEMENTS

The authors gratefully acknowledge the contributions of Bart Pierce who did most of the fixture preparation and proved to be indispensable during all phases of the experimental procedures. We thank Sharon Robinson for preparing and measuring many of the samples and Pat Kingman for the Back-reflection X-ray Topographic analysis of our samples.

1. INTRODUCTION

At the Ballistic Research Laboratory (BRL), a processing method has been developed to fabricate near full density TiB_2 and TiC structural ceramics. This technique utilizes an exothermic, combustion synthesis reaction also known as Self-Propagating High-Temperature Synthesis (SHS) to form a hot, porous, ceramic body. The reacted, still hot, body is consolidated to high density by the action of a pressure wave from the detonation of a high explosive, a method known as Dynamic Compaction (DC). This technique, designated as SHS/DC hereafter, has been applied in the fabrication of a variety of ceramic materials. A detailed description of this work is given by Niiler et al. (1988a, 1988b, to be published) and Benck et al. (1989).

The potential advantages of fabricating ceramics by SHS include self-purging of volatile contaminants caused by the high reaction temperatures and the possibility of forming unique material phases. A further advantage of the SHS/DC technique is that the use of explosives to consolidate the reaction product is potentially cost effective, especially for large sample sizes. However, the drawbacks associated with the method are the difficulties in eliminating cracking from the final product, providing sufficient insulation so the sample remains at a high temperature long enough for good intergrain bonding to occur, and the a priori prediction of the synthesis reaction behavior. A review of the SHS process and its characteristics can be found in a recent article by Munir (1988, 342-349).

The experiments of Niiler et al. (1988a, 1988b, to be published) established that the overall integrity of the ceramic product was predominantly dependent on the compatibility of reaction vessel properties and those of the compaction. It was found that the explosive charge thickness determined the product density which, in turn, controlled the product microhardness. Furthermore, the microstructures of the SHS/DC samples had significantly different grain sizes and morphologies different from those of equivalent hot-pressed materials. Both TiB_2 and TiC samples were successfully fabricated with product densities in excess of 98% of theoretical density (T.D.). However, the microhardness of the SHS/DC materials, especially that of TiC, was found to be lower than fully-dense hot-pressed materials.

Further experiments with TiB_2 and TiC were undertaken where the effects of precursor powder impurity levels on the TiB_2 and TiC product density, microhardness, and microstructure were of primary interest. In addition, the role of the impurities in the intergrain bonding and their effect on the dynamic consolidation process were evaluated. Since TiC is relatively stable over a wide range of carbon to titanium (C/Ti) atom ratios, the feasibility of producing TiC with varying C/Ti ratios was also investigated. Additionally, work was performed with ternary mixtures of titanium, carbon, and boron while attempting to produce TiC-TiB_2 composite structures using various TiB_2 to TiC (TiB_2/TiC) molar ratios. Some of the properties of the composite structures will be described.

2. EXPERIMENTAL PROCEDURE

Several types of precursor powders with different morphologies and purities were used to evaluate their effects on the product microstructure. The precursor powders are described in Table 1. All of the powders were examined with Scanning Electron Microscopy (SEM) and Energy Dispersive X-ray Analysis (EDS). They were dry-mixed under argon atmosphere and uniaxially pressed at 35 MPa into disc-shaped green compacts. Based on examination of the Ti-C phase diagram (Rudy, Brukl and Harmon 1965), the C/Ti ratio for the TiC samples was varied from 0.7 to 1.0. In the TiB_2 experiments, only the stoichiometric 2 to 1 ratio of boron to titanium (B/Ti) was used. The TiB_2/TiC ratio in the TiC-TiB_2 composites was varied from 0.00 to 0.43. In all of the ternary mixtures, a C/Ti ratio of 0.8 and B/Ti ratio of 2.0 was maintained.

The green compact was packaged in the reaction vessel, reacted, and, when the reaction was completed, the hot, porous reaction product was dynamically consolidated. A detailed description of the reaction vessel design and dynamic consolidation procedure has been reported by Niiler et al. (1988a) and Benck et al. (1989). The tests were carried out in reaction vessels designed to achieve complete consolidation of the reaction product, i.e., to produce full or near-full density samples. As previously determined by Niiler et al. (1988a, 1988b, to be published), complete consolidation required the use of c/m values (explosive charge mass to compression plate mass ratio) for the TiC tests of 0.44 and a

TABLE 1. Description of Precursor Powders.

Designation	*Size*	*Purity**	*Description*	*Manufacturer*
Ti-1	-325**	99.7	Titanium	Atlantic (1)
Ti-2	-325	99.5	Titanium	Micron Metals (2)
C-1	2 μm	99.9	Graphite	ConAstro (3)
C-2	0.05 μm	90.5	Carbon, Monarch 1300 90.5% fixed C content	Cabot (4)
C-3	0.05 μm	99.5	Carbon, Sterling R *99.5% fixed C content*	Cabot (4)
B-1	-325	99.5	Boron, crystalline	Atlantic (1)
B-2	-325	99.5	Boron, crystalline	Starck (5)
B-3	5 μm	96.5	Boron, amorphous	ConAstro (3)

* Manufacturer's Specified purity in percent.

** -325 mesh is equivalent to particle sizes less than 44 μm.

(1) Atlantic Equipment Engineers, Inc., Bergenfield, NJ.

(2) Micron Metals, Inc., Salt Lake City, UT.

(3) Consolidated Astronautics, Inc., Milwaukee, WI.

(4) Cabot Corporation, Boston, MA.

(5) Hermann C. Starck, New York, NY.

c/m value of 0.22 for the TiB_2 tests. The TiC-TiB_2 tests were performed with a c/m value of 0.29. The reacted and shock consolidated ceramic samples were approximately 1.2 cm thick with a diameter of 5.0 cm.

The effectiveness and uniformity of compaction in the ceramic disks was determined by density measurements and optical microscopy. A diamond cut-off saw or an electrical discharge machine was used to cut out the central region from the sample. The core samples were cleaned, and the mass density was measured by Archimedes' water immersion technique. These density measurements showed that, for 5.0 cm diameter disks, the central 2.5-3.0 cm "core" region was most uniformly compacted with a variation in density of about ± 0.5%. Circular cracks and delaminations were limited to the outer periphery of the disks.

Flat sections were cut from the core region for metallographic polishing. These pieces were potted with a thermosetting diallyl-phthalate resin compound. Due to the extreme hardness of the samples, only diamond grinding and polishing were found to be effective. The samples were first planed with a 600-mesh diamond grinding wheel and then sequentially polished on nylon polishing cloth with 6, 1, and 1/4 μm diamond sprays to a 1/4 μm finish. No further preparation of the polished cross-sections, such as etching or gold coating, was necessary for observation and analysis with optical or electron microscopy.

An optical microscopy evaluation of residual porosity levels and grain microstructure was followed by microhardness measurements. Hardness measurements were performed at room temperature using a Knoop indentor with both 100-g and 400-g test loads. With the 100-g test load, the indent usually extended over a single grain and thus was a measure of the material's single grain or intrinsic hardness. However, with the 400-g test load, the indent extended over several grains and thus indicated the material's overall or extrinsic hardness including grain boundary and porosity effects. The values reported here are averages from at least 15 individual measurements. The polished cross-sections and fracture surfaces from the sample were examined with SEM and EDS for grain structure, intergrain bonding, and impurity concentrations.

3. RESULTS AND DISCUSSION

During routine post-compaction evaluation of the SHS/DC ceramics, it was found that several of the samples contained iron in the grain boundaries. As iron and titanium can form relatively low melting point intermetallic phases, the presence of any iron in the samples has potentially serious consequences. The fact that the iron was segregated into the grain boundaries is also significant because a secondary component, in such locations, can ultimately determine the material's properties (Kny and Ortner 1986).

Since iron contamination from fixture sources external to the reacting green compact was excluded by the use of a sheet graphite barrier surrounding the sample, other sources of the iron had to be considered. Iron contamination may have been introduced by the precursor powders as steel equipment is commonly used in the size reduction and milling of

titanium powders. EDS and Inductively Coupled Plasma (ICP) analyses revealed that, in spite of quoted purity levels of 99.7%, some of the precursor powders were contaminated with much higher levels of iron. In the Ti-1 powder (see Table 1) the iron impurity varied from approximately 1 wt% to 3 wt%, lot to lot. The B-1 boron powder was also found to contain a similar, high level of 3 wt% of iron. Subsequently, other titanium and boron powders were obtained, namely Ti-2 and B-2, and with ICP analysis they were found to contain a minimal amount of 0.1 wt% iron. The amorphous boron contained less than 0.1% iron. SEM analysis indicated that the two crystalline boron powders, B-1 and B-2, had equivalent particle morphologies and size distributions. The two titanium powders, Ti-1 and Ti-2, also were found to have equivalent morphologies and size distributions. The effects of the iron and other impurities on the SHS/DC processed TiB_2 and TiC, as well as the effect of variation of the C/Ti ratio on TiC, are discussed in the following sections.

3.1 <u>TiB_2</u>. As reported previously, the crystal structure of SHS/DC TiB_2 is polycrystalline with individual crystals forming from a melt (Niiler et al. 1988a). This is due to the fact that the combustion synthesis process produces temperatures in excess of the melting temperatures of both the precursors and the product TiB_2. With the addition of the frictional heating associated with the dynamic consolidation process, the fully dense product is homogenized and possibly remelted. This resulting structure is different from the structures of various TiB_2 materials produced by hot-pressing techniques. The hot-pressed TiB_2 structures usually consist of equiaxed, polycrystalline grains with some type of sintering aid still present in the grain boundaries.

Figure 1 shows backscattered electron photomicrographs of four TiB_2 samples. A commercial, hot-pressed (CHP) sample is shown in Figure 1A and three SHS/DC TiB_2 samples (DC1, DC2, and DC3) are shown in Figures 1B, 1C, and 1D, respectively. Sample DC1 was made with the iron-free crystalline boron (B-2) and iron-free titanium (Ti-2) precursors. Sample DC2 was made with the iron contaminated precursors, B-1 and Ti-1, while sample DC3 was made with the amorphous boron precursor (B-3) and the iron-contaminated Ti-1 precursors. The density and microhardness results for the TiB_2 samples are summarized in Table 2. The sample densities were normalized to the theoretical density of TiB_2, 4.50 g/cm^3. The bright areas in Figure 1 are various impurity rich phases, the light-gray areas are TiB_2 grains, and the dark-gray areas are closed pores. A

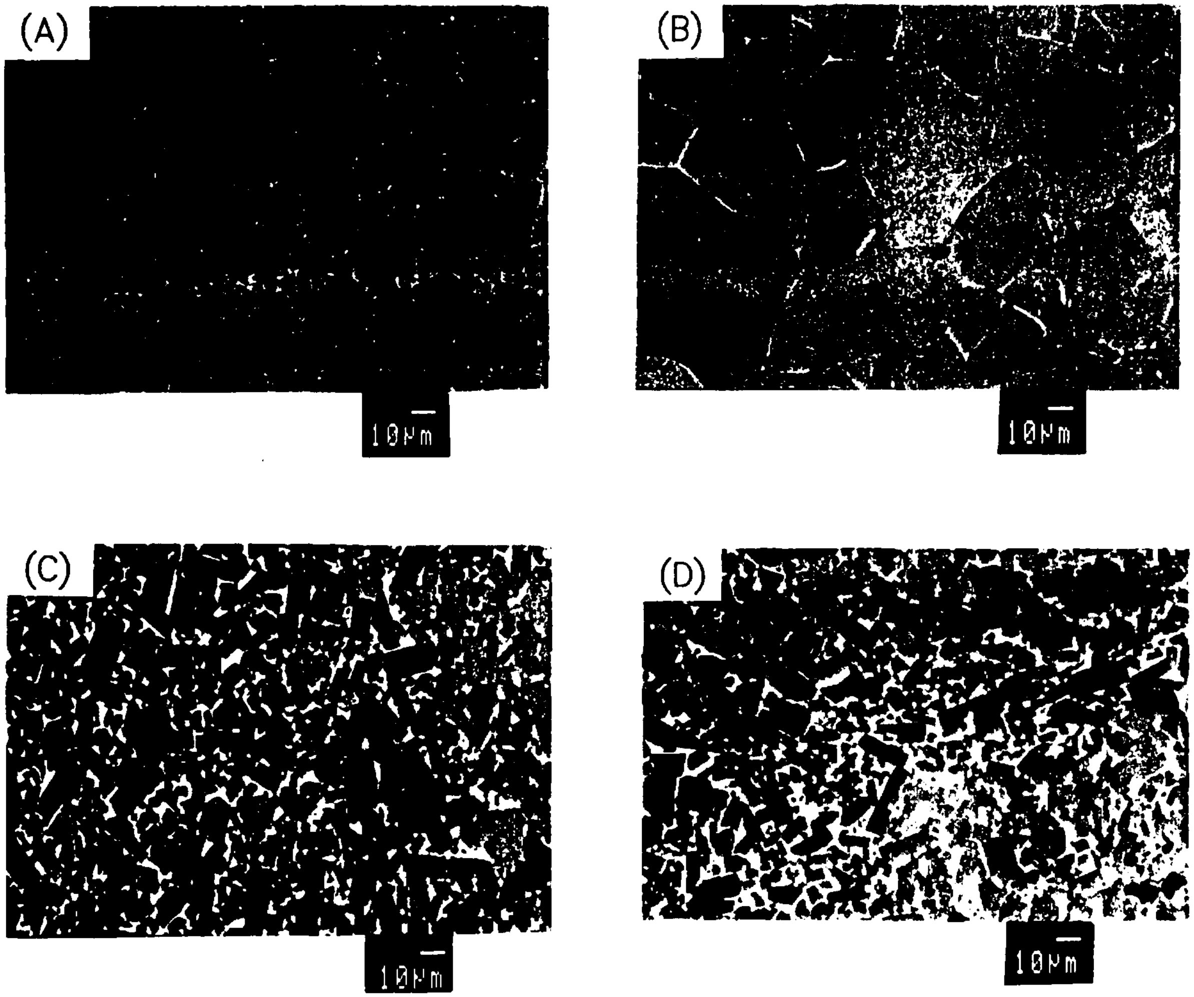

Figure 1. Polished Cross-Sections of TiB_2. Hot-Pressed TiB_2 Sample in 1A; SHS/DC Samples DC1 (Iron-Free Precursors) in 1B, DC2 (Iron-Contaminated Precursors) in 1C, and DC3 (Amorphous Boron and Iron-Contaminated Titanium Precursors) in 1D.

TABLE 2. TiB_2 Results.

Sample	Density (% T.D.)	Microhardness HK (100 g) (GPa)	Microhardness HK (400 g) (GPa)
CHP	98+	33.6 ± 1.3	21.4 ± 1.1
DC1	98.0	34.6 ± 0.8	22.4 ± 0.6
DC2	98.0	32.6 ± 1.3	23.5 ± 0.5
DC3	91.6	26.4 ± 1.4	17.5 ± 0.8

comparison of the DC3 and DC2 samples reveals the effect of the type of boron used, and a comparison of the DC2 and DC1 samples reveals the effect of iron on the microstructure.

Due to the large volume of volatile impurities on the B-3 powder, the residual porosity in the DC3 sample is high. In contrast, both samples made with crystalline boron have little residual porosity. The hypothesis that a portion of the TiB_2 melts under these conditions is supported by the micrographs of polished surfaces of the TiB_2 samples. The DC2 and DC3 sample surfaces show grain shapes which are consistent with a section cut through randomly oriented, hexagonal single crystal grains. This single crystal formation could only occur during cool-down from a molten phase of TiB_2. TiB_2 crystals cannot be seen by electron microscopy in the DC1 sample which was made from clean precursors. However, back reflection X-ray topographs (Kingman, private communication) reveal the presence of a sub-grain structure. Consequently, it may be concluded that in the absence of iron, the TiB_2 single crystals in the DC1 sample were able to spatially grow continuously, merging together into larger grains. The DC2 and DC3 samples clearly show that the presence of iron tends to arrest the growth of the TiB_2 grains.

EDS analysis indicates that, in the SHS/DC samples, the iron impurity is limited to the grain boundaries and is not detected within the TiB_2 grains. Grain boundary regions of the DC2 and DC3 samples show large amounts of iron. Only minute quantities of iron are present in the grain boundaries of the DC1 sample. The bright regions of the hot-pressed TiB_2 sample contain cobalt, a known sintering aid in the hot-pressing of this TiB_2.

Room temperature fractographs show that both porosity and the iron impurity reduce

intergrain bonding. Backscattered electron photomicrographs of the four TiB_2 samples are shown in Figure 2. While in the DC1 sample (see Figure 2B), the failure is by transgranular fracture only, in the other samples (including the hot-pressed TiB_2) failure occurs by both intergranular and transgranular fracture. Since the 100-g microhardness values are about the same (see Table 2), the increased number of intergranular fracture sites in these samples indicates a reduction in the quality of intergranular bonding.

As shown in Table 2 for TiB_2, a 98.0% T.D. has been achieved with the use of both crystalline boron powders. When examining the density of the DC2 sample, the effect of the iron found on the Ti-1 and B-1 precursors must also be considered. The 3 wt% iron impurity on these precursors is responsible for about a 1% increase in the overall sample density. The use of amorphous boron in the DC3 sample results in a reduction of about 6% in density. This lower density is due to the larger volume of volatile contaminants on the boron being expelled from the sample during the synthesis reaction, causing channels and voids that do not heal under compaction. The particle size may also be a factor since the smaller amorphous particles will result in a higher combustion rate and thus a more violent expulsion of the impurities. Although the SHS/DC TiB_2 samples are only 98.0% T.D., their microhardness values are equivalent to, if not better than, the hot-pressed sample. The lower hardness values of the DC3 sample with amorphous boron is caused by its high porosity. Specifically, the porosity is so well distributed that there are very few fully dense regions where a hardness measurement could be made without the collapse of adjacent grains.

3.2 TiC. Like other Group IVA carbides, titanium carbide is the only intermediate phase in the titanium-carbon binary system. The carbide has an interstitial NaCl crystal structure that is stable from C/Ti ratios of 0.65 up to the stoichiometric composition. TiC has a maximum melting temperature at a C/Ti value of 0.88, below the stoichiometric composition (Munir 1988, 342-349). Previous investigations have demonstrated that the properties of TiC depend strongly on the C/Ti ratio (Toth 1971; Miracle and Lipsitt 1983, 592-597; Storms 1967; Yamada, Miyamato and Koizumi 1987, c206-c208). The fabrication of TiC with different C/Ti ratios is very convenient and straightforward with the SHS/DC

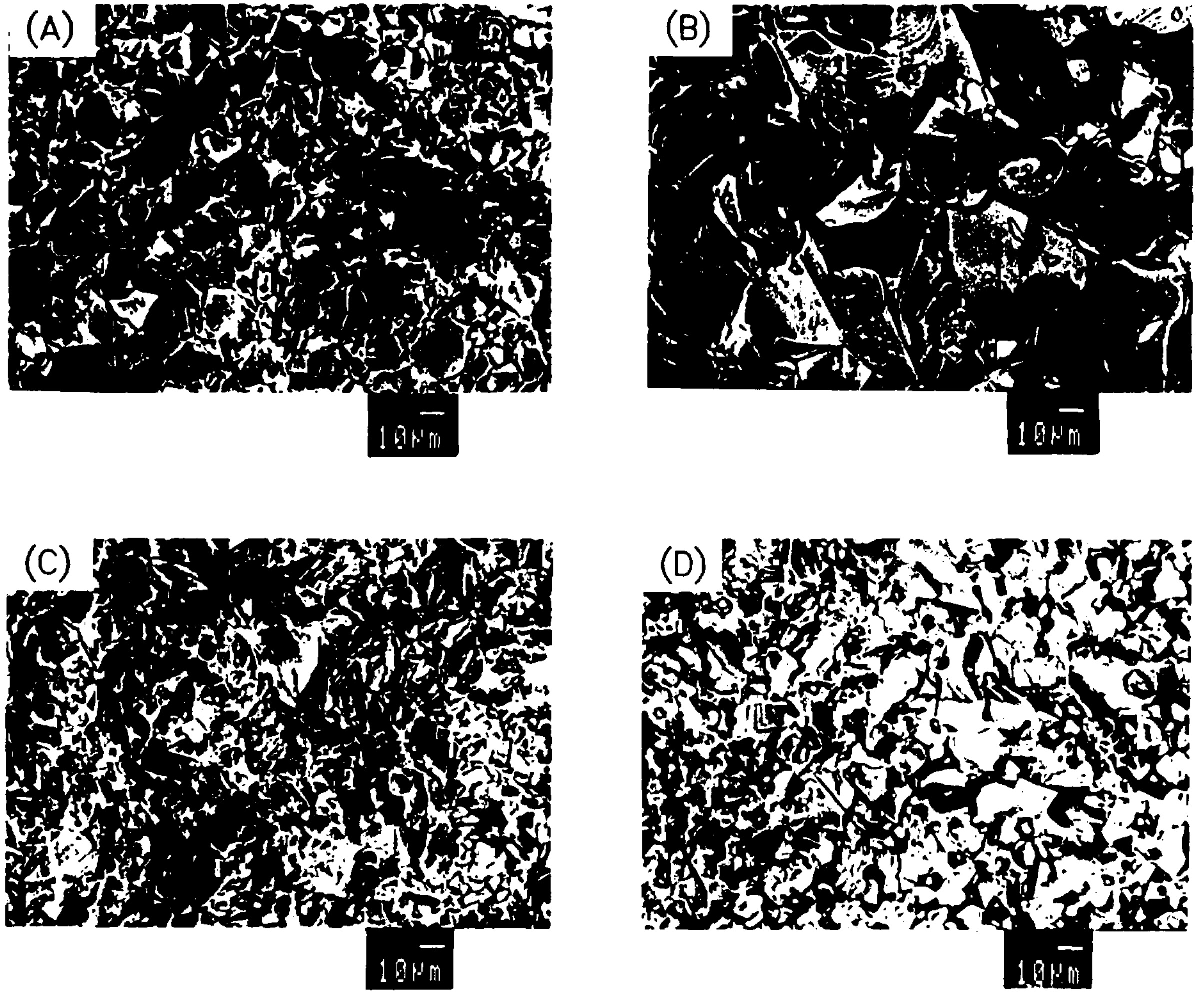

Figure 2. Fractographs of TiB_2. Hot-Pressed TiB_2 Sample in 2A; SHS/DC Samples DC1 (Iron-Free Precursors) in 2B, DC2 (Iron-Contaminated Precursors) in 2C, and DC3 (Amorphous Boron and Iron-Contaminated Titanium Precursors) in 2D.

processing method. Consequently, in addition to examining the effects of the iron on the product structure, TiC samples with a range of C/Ti ratios from 0.7 to 1.0 were also prepared and analyzed.

3.2.1 Effect of Iron Impurity. The effect of the iron impurity on the TiC microstructure is shown in the backscattered electron photomicrographs of Figure 3 which show the three SHS/DC samples, DC4 (3B), DC5 (3C), and DC6 (3D), along with a hot-pressed TiC sample (3A). Sample DC4 was made with the iron-free titanium (Ti-2) and the graphite (C-1) precursors. Sample DC5 was made with the iron-contaminated titanium (Ti-1) and the graphite (C-1) precursors, while Sample DC6 was made from the iron-contaminated titanium (Ti-1) and the carbon black (C-2) precursors. The density and microhardness results for the TiC samples are summarized in Table 3. The sample densities were normalized to the theoretical density of TiC, 4.93 g/cm^3.

TABLE 3. TiC Results.

Sample	Density	C/Ti Ratio	Microhardness	
	(% T.D.)		HK (100 g)	HK (400 g)
			(GPa)	
CHP	98+	1.0	25.5 ± 0.6	19.4 ± 0.5
DC4	93.1	0.8	20.4 ± 0.6	16.3 ± 0.4
DC5	97.3	0.8	21.4 ± 0.6	17.3 ± 0.6
DC6	98.0	0.8	20.4 ± 0.6	16.3 ± 0.4

In the samples of Figure 3, the bright areas are the iron-rich impurity phases, the light-gray areas are TiC grains, and the dark-gray areas are closed pores. Comparison of the DC5 and DC6 samples reveals the effects of the carbon precursor, while comparison of the DC4 and DC5 samples reveals the effect of iron on the sample microstructure. The SHS/DC TiC grain morphology differs from that of TiB_2, consistent with the TiC grains being

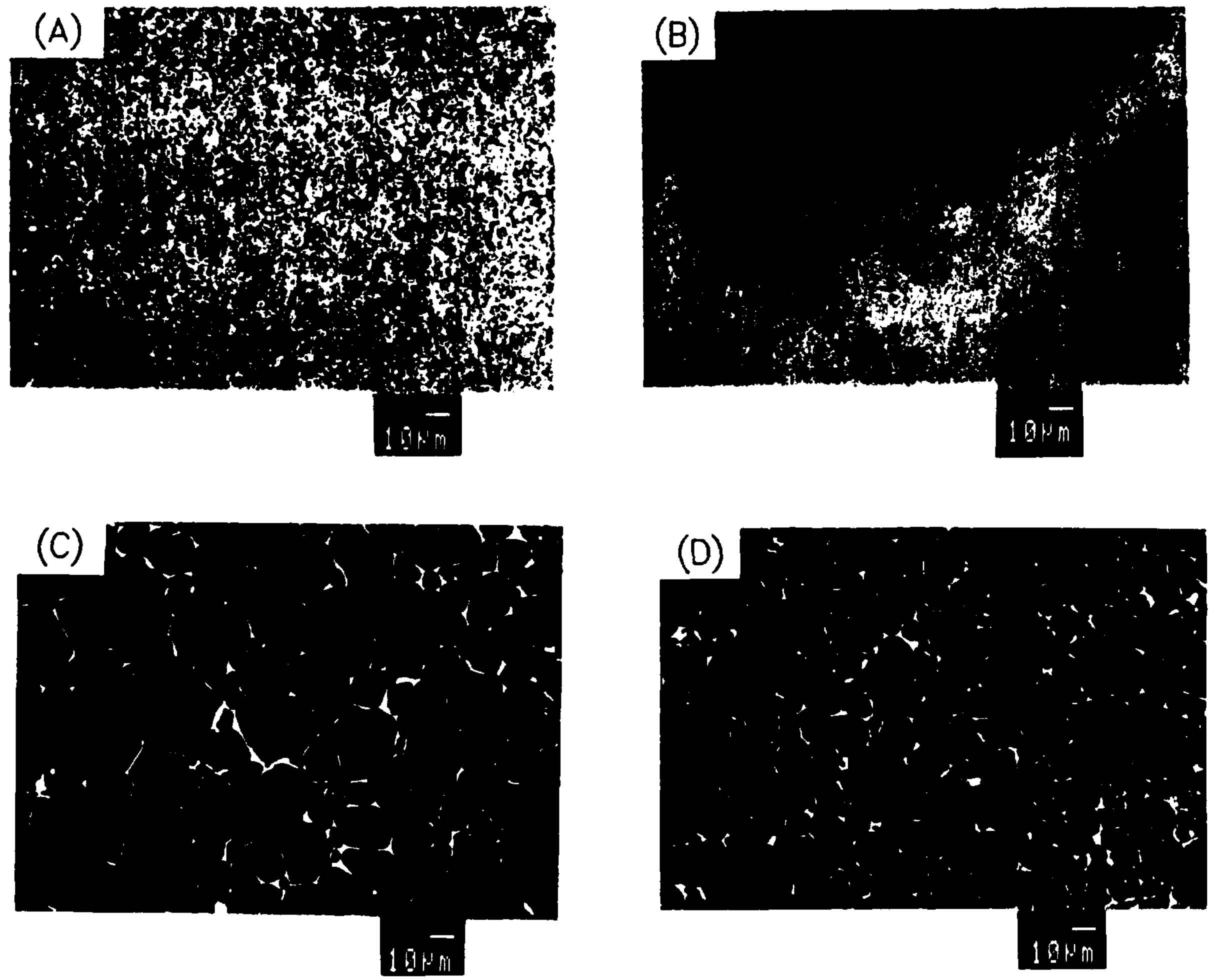

Figure 3. Polished Cross-Sections of TiC. Hot-Pressed TiC Sample in 3A; SHS/DC Samples DC4 (Iron-Free Titanium and Graphite Precursors) in 3B, DC5 (Iron-Contaminated Titanium and Graphite Precursors) in 3C, and DC6 (Iron-Contaminated Titanium and Carbon Black Precursors) in 3D.

plastic but at temperatures below the TiC melting point. Additionally, the residual level of the iron impurity significantly influences sintering and the grain morphology of the material. Each of these factors is discussed in more detail below.

The grain morphology of the SHS/DC TiC samples consists of equiaxed, plastically deformed grains. The grain size in the DC5 sample is approximately twice as large as the grain size in the DC6 sample. This is a result of the respective grain sizes of the graphite and carbon black particles. Specifically, the 2 μm graphite flakes tend to agglomerate into 10-20 μm clumps, whereas the submicron carbon black agglomerates into smaller 10 μm clumps. Although the faint grain contrast in the DC4 sample makes observation difficult, the grain morphology is similar to that of the DC5 sample. The residual porosity in the DC5 and DC6 samples appears to scale with the respective grain sizes. In particular, the size of the triple junctions formed between larger grains tend to be larger than those between smaller grains. The residual porosity of the DC4 sample, however, is well dispersed and extremely fine.

EDS analysis of the samples and the precursor powders indicates that many of the impurities found on the precursor powders remain in the product. This is significant because at the reaction temperatures (2000-2500°C), even "non-volatile" impurities (e.g. iron) have sufficiently high vapor pressures (10-100 torr) that could allow their evolution from the product. However, in all of the SHS/DC samples, the impurities are limited to the grain boundaries only and are not detected within the TiC grains. Only titanium and iron are seen in the grain boundaries of the DC5 sample. As is apparent from the lack of atomic number phase contrast in the DC4 sample, no impurities could be detected. The bright regions in the hot-pressed TiC sample contain tungsten and are probably WC. As discussed in the TiB_2 section earlier, the iron impurity on the Ti-1 powder also remains in the SHS/DC TiC samples. The amount of iron in the DC5 and DC6 samples was approximately 2.5 wt%. Analyses of grain boundary regions of the DC6 sample show the elements titanium, sulfur, and chlorine in addition to iron. The source of the sulfur and chlorine is the C-2 carbon black powder used in its fabrication, as verified by EDS and vacuum outgassing experiments (Kecskes and Niiler 1989, 655-661) with this powder.

The residual impurities remaining in the samples affect the characteristic failure mode of TiC. Figure 4 shows room temperature fractographs of the hot-pressed and the three

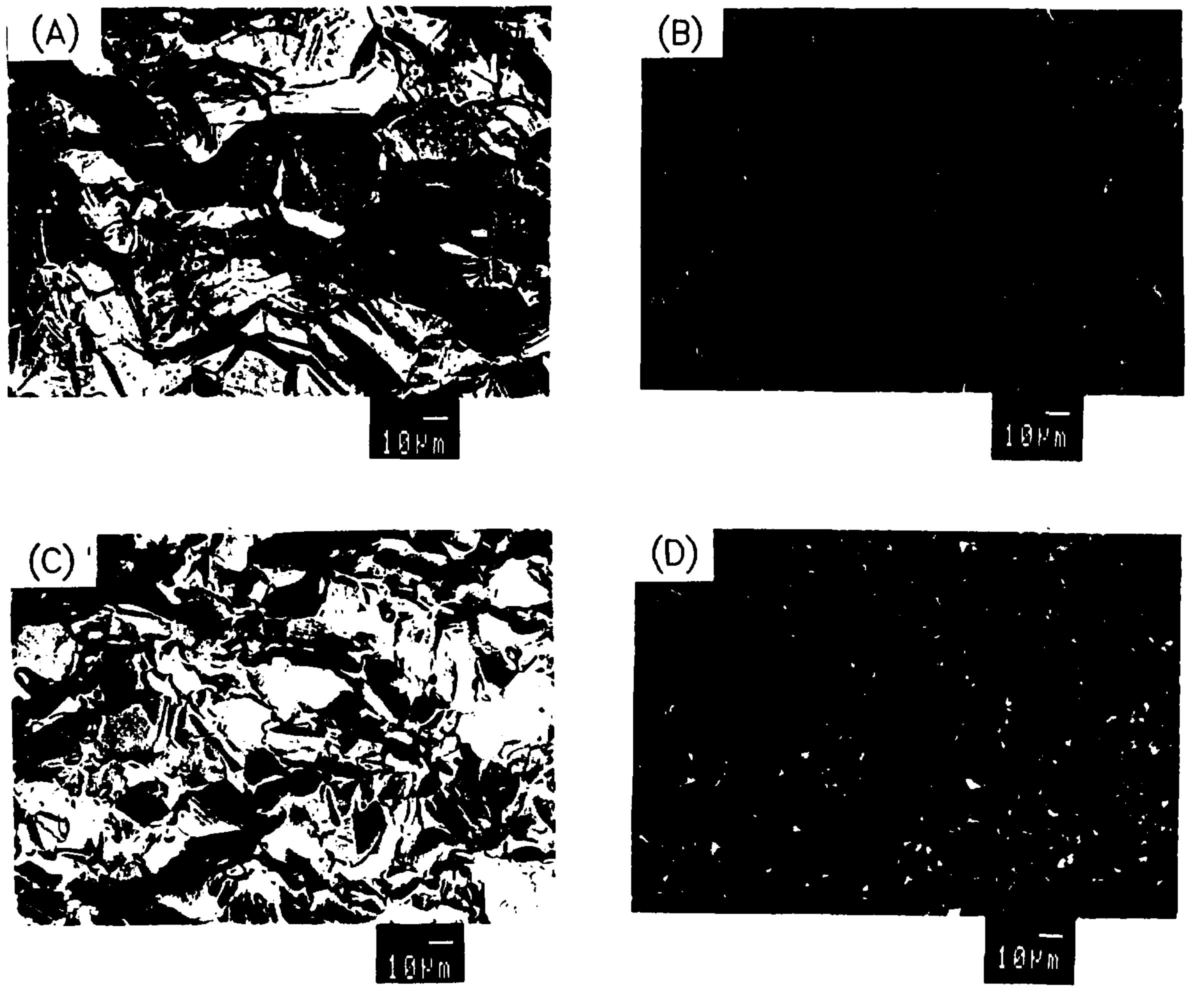

Figure 4. Fractographs of TiC. Hot-Pressed TiC Sample in 4A; SHS/DC Samples DC4 (Iron-Free Titanium and Graphite Precursors) in 4B, DC5 (Iron-Contaminated Titanium and Graphite Precursors) in 4C, and DC6 (Iron-Contaminated Titanium and Carbon Black Precursors) in 4D.

SHS/DC TiC samples. The hot-pressed sample fails by transgranular fracture only. In contrast, the relatively lower fracture strength of the SHS/DC samples is indicated by the fact that, in these samples, failure occurs by both transgranular and intergranular fracture. Additionally, it may be noted that the 100-g hardness measurements of individual grains are lower for the SHS/DC samples than the hot-pressed sample. Based on the number of intergranular fracture sites and the 100-g microhardness measurements, the intergrain bonding in the DC4 sample is probably the weakest while the bonding in the DC5 sample might be the strongest. It is believed that the use of "iron-free" powders in the DC4 sample eliminates the iron impurity that otherwise acts as a binder (Ramqvist 1965, 2-21) between grains and contributes to room temperature strength.

The segregation of impurities to grain boundaries is generally undesirable, but the presence of a low melting point metal binder in the SHS/DC TiC samples evidently aids the densification process. This effect was observed by Riley (Riley and Niiler 1987) in the low pressure compaction of TiB_2 and TiC and is already used in the Soviet Union to produce cermet cutting tools (Merzhanov et al. 1980). As seen in Table 3, the DC5 and DC6 sample densities are approximately 4 to 5% higher than that of DC4 and comparable to the density of the hot-pressed sample. As was the case with TiB_2, the effect of the 2.5 wt% iron impurity on the overall DC5 and DC6 sample densities is only about 1%. Therefore, the presence of small amounts of a low temperature melting point phase significantly enhances the densification. Another indication of the enhanced densification process can be observed in the residual porosity of the samples (see Figure 3). The pores in both iron-contaminated samples are predominantly at grain triple junctions. However, in the case of the iron-free sample, the residual porosity is uniformly dispersed. It is speculated that when the hot, porous SHS product is consolidated, the iron-rich phase remains molten, and when the porosity is squeezed out of the bulk, the melt acts as a carrier of isolated pores. The molten phase also reduces friction between TiC grains, thereby improving the overall densification process.

Although the iron may be a lubricating agent during compaction, it does not appear to affect the sample microhardness at room temperature. This can be seen from Table 3, where all three SHS/DC samples show similar microhardness values. The lower microhardness values of the SHS/DC samples compared to that of the hot-pressed sample

are a result of the C/Ti ratio of 0.8 used in these experiments (Niiler et al. 1988a). The results of experiments where the effect of the C/Ti ratio on sample properties were investigated are described next.

3.2.2 Effect of C/Ti Ratio. The effects on product density of varying the C/Ti ratio from 0.7 to 1.0 are shown in Figure 5. This figure (5A) shows that the SHS/DC TiC sample density is maximum for C/Ti of 1.0 and drops off for lower ratios. The theoretical mass density of TiC is indicated by the solid line. However, when the ratio of the experimental data to the theoretical value, i.e., percent T.D., is plotted, an interesting feature of the SHS/DC process becomes evident (see Figure 5B). At lower C/Ti ratios, the samples are closer to their full density. In other words, densification with dynamic consolidation becomes more effective with decreasing C/Ti ratios. It is speculated that as the C/Ti ratio decreases, the increasing number of carbon vacancies results in less restrictive motion of the dislocations and thus easier deformation of the TiC grains.

Microhardness measurements of the SHS/DC and hot-pressed TiC samples are plotted in Figure 6. The 100-g values for the stoichiometric composition SHS/DC sample exceed that of the commercial, hot-pressed sample. The 100-g microhardness above a C/Ti ratio of 0.95 remains constant, but below 0.95 the hardness steadily decreases with decreasing C/Ti ratio. At 400-g, the SHS/DC microhardness is essentially the same as that of the hot-pressed sample, reaching a maximum at C/Ti of 0.95, and then decreasing. These 400-g tests suggest that as C/Ti ratios near 1.0, the intergranular bonds in the SHS/DC samples are weakened. Additionally, as is evident from the figure and Table 3, the hardness values of the DC4, DC5, and DC6 samples with a C/Ti of 0.8 fit the C/Ti ratio dependence of TiC quite well.

SEM analyses of the TiC samples revealed a striking change in the characteristic porosity and fracture mode with changing C/Ti ratios. Figure 7 shows backscattered electron images of polished cross-sections from the hot-pressed TiC sample and the SHS/DC TiC samples. It may be noted that for these samples, which were formed from iron-free precursor powders, the grain to grain-boundary contrast observed with iron-laden powders is absent. The lack of contrast also demonstrates that all of the precursors have been consumed in the SHS reaction, and no precursor remants, such as unreacted titanium or carbon, remain in the product. In Figure 7A, the structure of grain triple junctions that arises from incomplete deformation of close-packed grains is well preserved in the residual

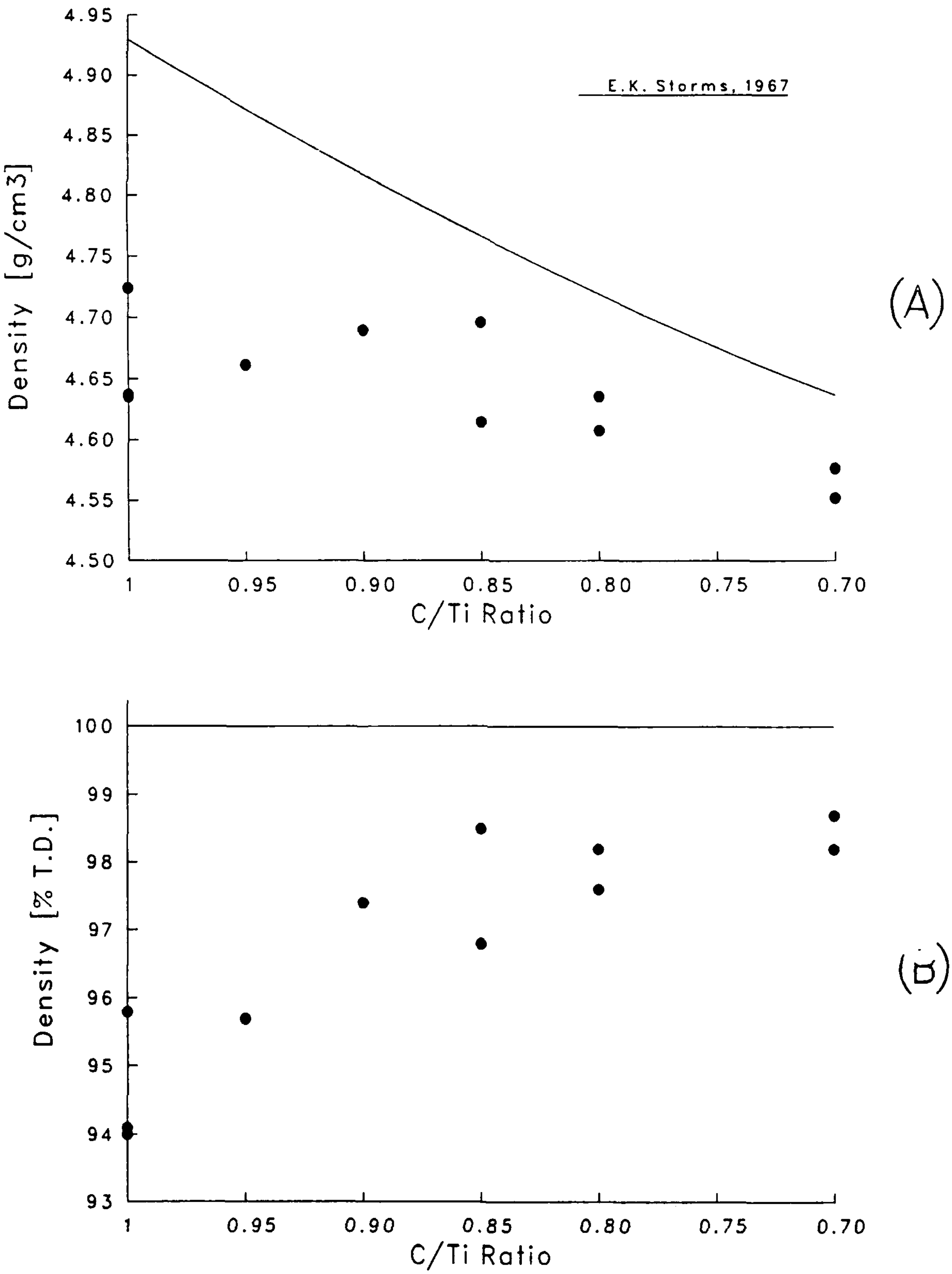

Figure 5. Density Dependence of TiC. Mass Density vs. C/Ti Ratio in 5A and Percent T.D. vs. C/Ti Ratio in 5B.

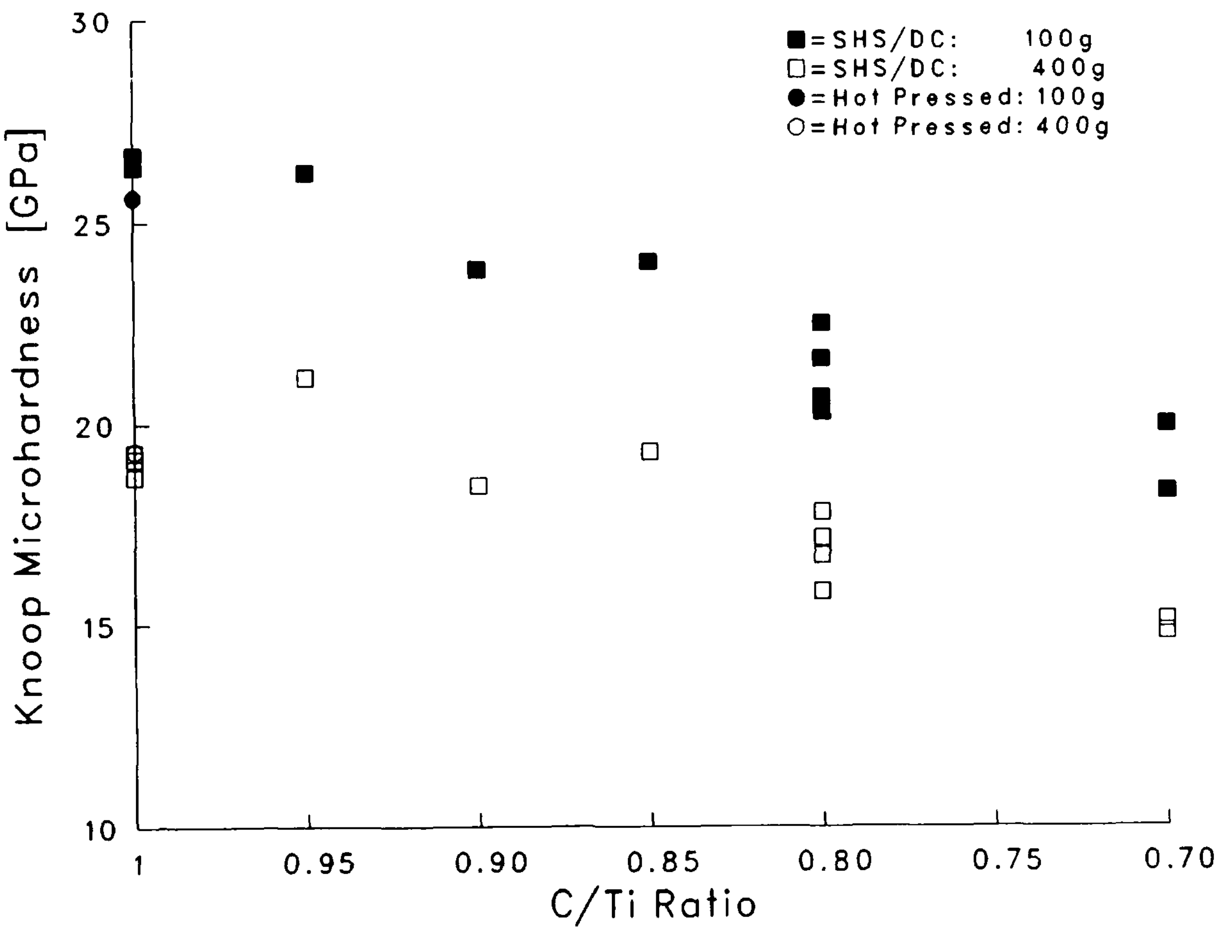

Figure 6. <u>TiC Sample Microhardness vs. C/Ti Ratio</u>.

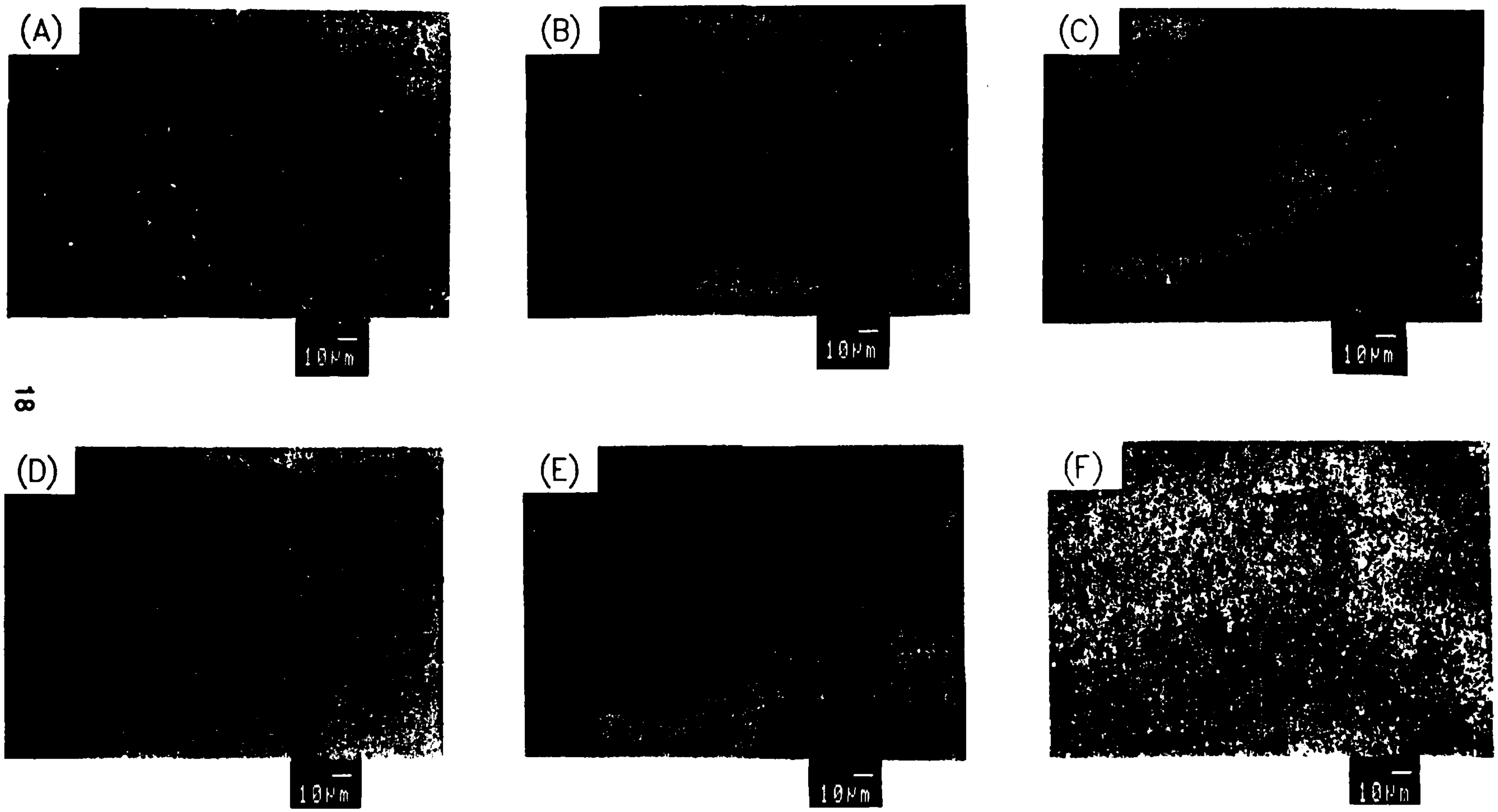

Figure 7. <u>Polished Cross-Sections of TiC with C/Ti of 1.0 in 7A, 0.95 in 7B, 0.9 in 7C, 0.8 in 7D, 0.7 in 7E, Hot-Pressed in 7F</u>.

porosity. As seen in Figures 7B and 7C, when the C/Ti ratio is decreased to 0.95 and 0.9, the triple junctions between grains begin to round and are eventually closed out of the bulk. However, when the C/Ti ratio is further decreased to 0.8 and 0.7, as shown in Figures 7D and 7E, another type of porosity which is extremely fine and evenly distributed throughout the material becomes dominant. A possible explanation for the appearance of this type of porosity will be discussed later.

Room temperature fractographs of the TiC samples show a generally mixed fracture mechanism. Figure 8 shows backscattered electron images of representative fracture surfaces from the TiC samples. Although the hot-pressed TiC has a relatively larger grain size, the failure mode of the SHS/DC sample with C/Ti of 1.0 is essentially the same. The failure mechanism changes from a predominantly transgranular fracture at C/Ti of 1.0 to intergranular fracture at C/Ti of 0.7. The uniformly dispersed porosity of the TiC samples with C/Ti of 0.8 and 0.7 in Figures 7D and 7E is indicative of increasing concentrations of trapped volatile impurities. These impurities remain in the bulk because, at lower C/Ti ratios, there is less heat available to drive them out. Thus, the change in the failure mode is probably related to less heat energy being produced by the TiC reaction as the C/Ti ratio is decreased. Furthermore, with less heat at lower C/Ti ratios, sintering is also reduced, resulting in weaker intergrain bonds. The failure mode of TiC may also explain the turnover in the 400-g hardness curve. SEMs of hardness indents show that at C/Ti of 1.0, the TiC grains are so hard and brittle that when the hardness indent is made, rather than plastically deforming to accommodate the indentor, the grains actually fracture and break up.

3.3 $\underline{TiC\text{-}TiB_2}$. The $TiC\text{-}TiB_2$ composite system was investigated primarily in order to combine the desirable properties of the TiC and the TiB_2 SHS/DC processes. The TiC SHS reaction is gentler, but TiC requires more effort to compact. In contrast, the TiB_2 product is easier to consolidate, but the reaction is more violent. Therefore, it was postulated that a $TiC\text{-}TiB_2$ mixture may produce a controlled SHS reaction with a product that is easier to dynamically consolidate. Consequently, an intermediate c/m ratio was selected between the c/m needed to consolidate TiC and the c/m needed to consolidate TiB_2.

Three $TiC\text{-}TiB_2$ composites were fabricated, with TiB_2/TiC ratios of 0.11 in the DC7 sample, 0.25 in the DC8 sample, and 0.43 in the DC9 sample. For comparison, a pure TiC sample, DC10, was also prepared under the same conditions as the composites. In the

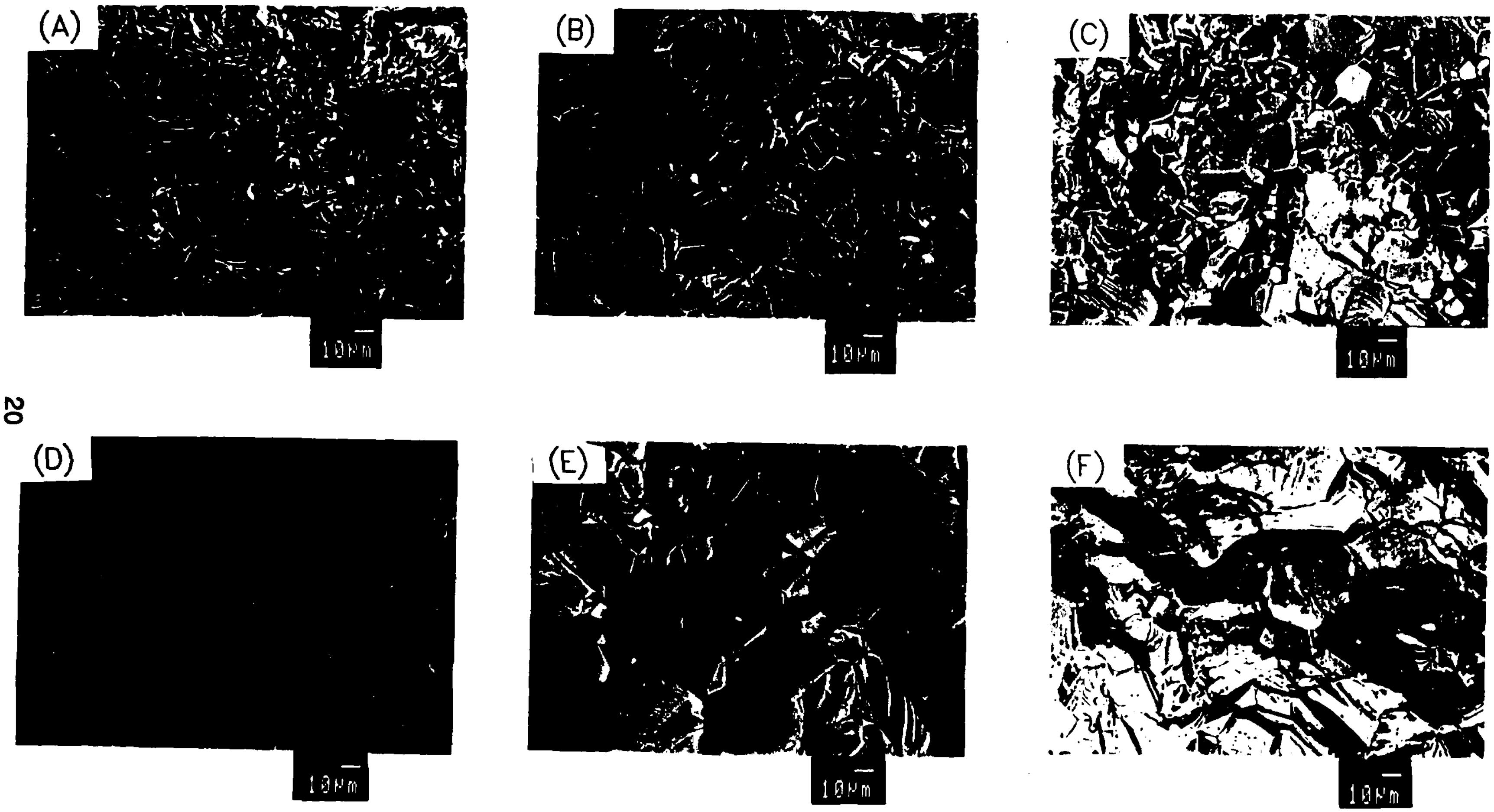

Figure 8. Fractographs of TiC with C/Ti of 1.0 in 8A, 0.95 in 8B, 0.9 in 8C, 0.8 in 8D, 0.7 in 8E, Hot-Pressed in 8F.

fabrication of these samples, the iron-contaminated powders Ti-1, B-1, and another carbon black, C-3, were used. An additional sample, DC11, was also prepared with a TiB_2/TiC ratio of 0.25 using the iron-free Ti-2, B-2, and C-1 powders. The sample densities and microhardness values are shown in Table 4. The density of each sample was normalized to the corresponding theoretical density of the composite.

TABLE 4. TiC-TiB_2 Results.

Sample	Density (% T.D.)	TiB_2/TiC Ratio	Microhardness (GPa) HK (100 g)	HK (400 g)
DC10	94.1	0.00	21.5 ± 0.6	15.5 ± 0.4
DC7	92.4	0.11	21.2 ± 0.7	16.7 ± 0.5
DC8	91.5	0.25	23.0 ± 0.8	16.6 ± 0.5
DC11	87.5	0.25	20.6 ± 0.4	15.8 ± 0.4
DC9	94.1	0.43	20.7 ± 1.0	16.6 ± 0.6

3.3.1 Effect of Iron Impurity. Backscattered electron images of polished cross-sections of the DC11 (iron-free) and DC8 (iron-contaminated) samples are shown in Figure 9. The micrographs reveal a highly heterogeneous system where both the TiC and TiB_2 phases can be readily distinguished. The light-gray areas are TiC, the dark-gray areas are TiB_2, and the black areas are closed pores. In the DC8 sample, the bright areas between grains correspond to the iron impurity phase. Suprisingly, the TiB_2 phase consists of randomly oriented single-crystal grains that are identical in appearance to the single crystals found in pure SHS/DC TiB_2, while the TiC grains appear to be the same as those found in pure SHS/DC TiC. Although excess titanium powder was used to synthesize the SHS products, as is evident in the figure, only TiC and TiB_2 were formed. In other words, the composite consists of a pseudo-binary mixture of TiB_2 single crystals or crystal aggregates spread through a TiC matrix. This is significant because it implies that, as was observed in the experiments with TiC, the SHS reaction consumes all of the reactants to form stable, if not stoichiometric, end-products. It may be noted that this feature is attributed to the high stability of the TiC lattice.

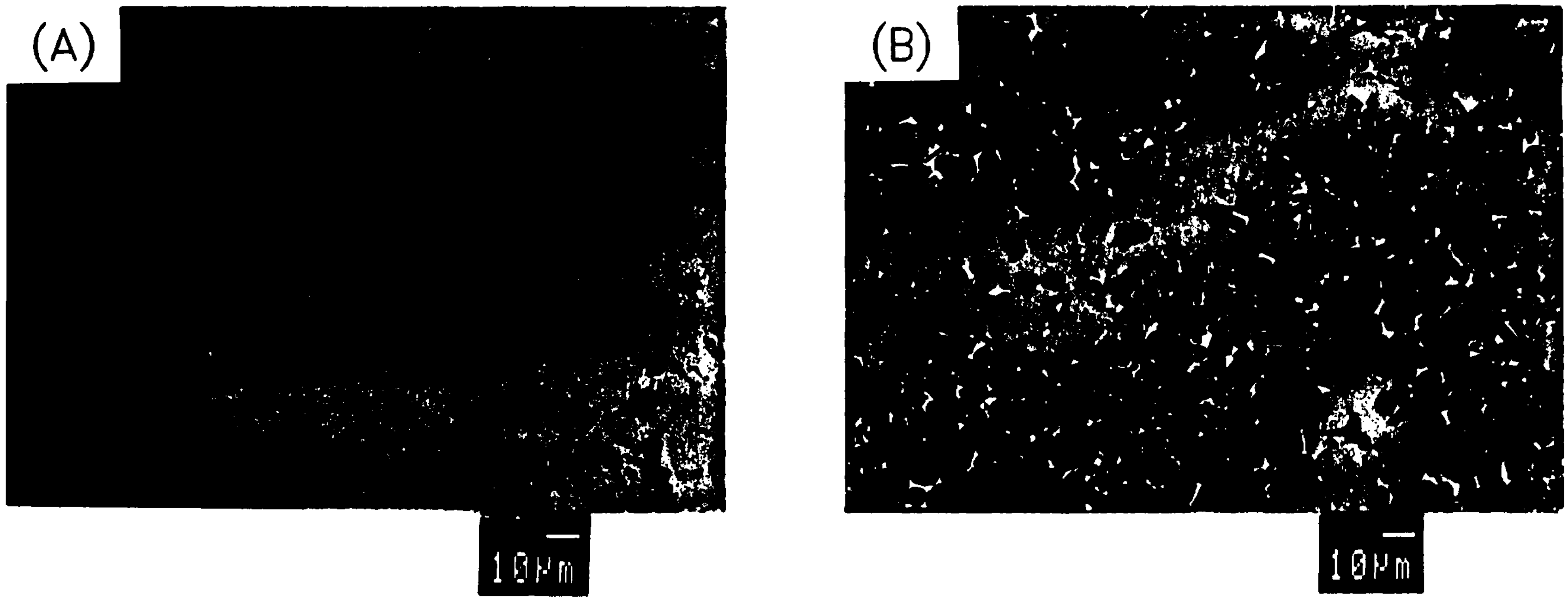

Figure 9. Polished Cross-Sections of SHS/DC TiC-TiB_2 Composites with a TiB_2/TiC Ratio of 0.25. Sample DC11 (Iron-Free) in 9A and Sample DC8 (Iron-Contaminated) in 9B.

The presence of iron appears to strongly alter the microstructural appearance of the $TiC-TiB_2$ composites. As evident in Figure 9, the TiB_2 phase seen in the iron-contaminated DC8 sample appears either as individual crystals forming between adjacent TiC grains or as parts of larger aggregates. The aggregation of the crystals is probably caused by a nonuniform and incomplete dispersion of the boron powder in the titanium-carbon powder mixture. With the iron impurity absent in the DC11 sample, the dispersion of the crystals is somewhat improved. The more immediate mixing of the two phases is demonstrated by other microstructural features absent in the DC8 sample. As can be seen in the upper left portion of Figure 9A, there are whisker-like TiB_2 structures a few microns thick and 20-30 µm long. A careful examination reveals that these crystallites are actually hexagonal TiB_2 platelets. Randomly oriented stacks of such TiB_2 platelets appear to alternate and mix with similar size TiC layers. It is speculated that in the absence of the iron impurity phase, the molten TiB_2 phase can readily penetrate and crystallize between the loosely stacked graphitic TiC layers during the SHS reaction.

The room temperature fracture surfaces of the DC8 and DC11 samples are shown in Figure 10. Both samples fail with a mixed mode, intergranular and transgranular fracture. Because the characteristic failure modes appear similar in the samples, the effect of the iron impurity on the mechanical properties is difficult to ascertain. Additionally, as seen in Table 4, the DC8 sample microhardness is similar to that of the DC11 sample. This suggests that while the iron binder was found to contribute to room temperature strength in the pure ceramics, its role is diminished by the presence of the secondary TiB_2 phase in the composite. Nevertheless, as observed earlier with TiC and TiB_2, the use of iron-contaminated precursors improves the densification process and results in a 4% increase in the density of the DC8 sample.

3.3.2 Effect of TiB_2/TiC Ratio. Backscattered electron images of polished cross-sections from the SHS/DC $TiC-TiB_2$ samples are shown in Figure 11 with the DC10 (TiC only) sample in 11A, DC7 (TiB_2/TiC = 0.11) sample in 11B, DC8 (TiB_2/TiC = 0.25) sample 11C, and DC9 (TiB_2/TiC = 0.43) sample in 11D. As expected, with increasing amounts of TiB_2 in the product, the TiB_2 crystal aggregates also increase in size. The residual porosity of the samples is bimodal. With only TiC present, the porosity consists of uniformly dispersed, isolated pores that are limited to grain triple junctions and grain boundaries. As TiB_2 is introduced to form the composite, a second, much larger,

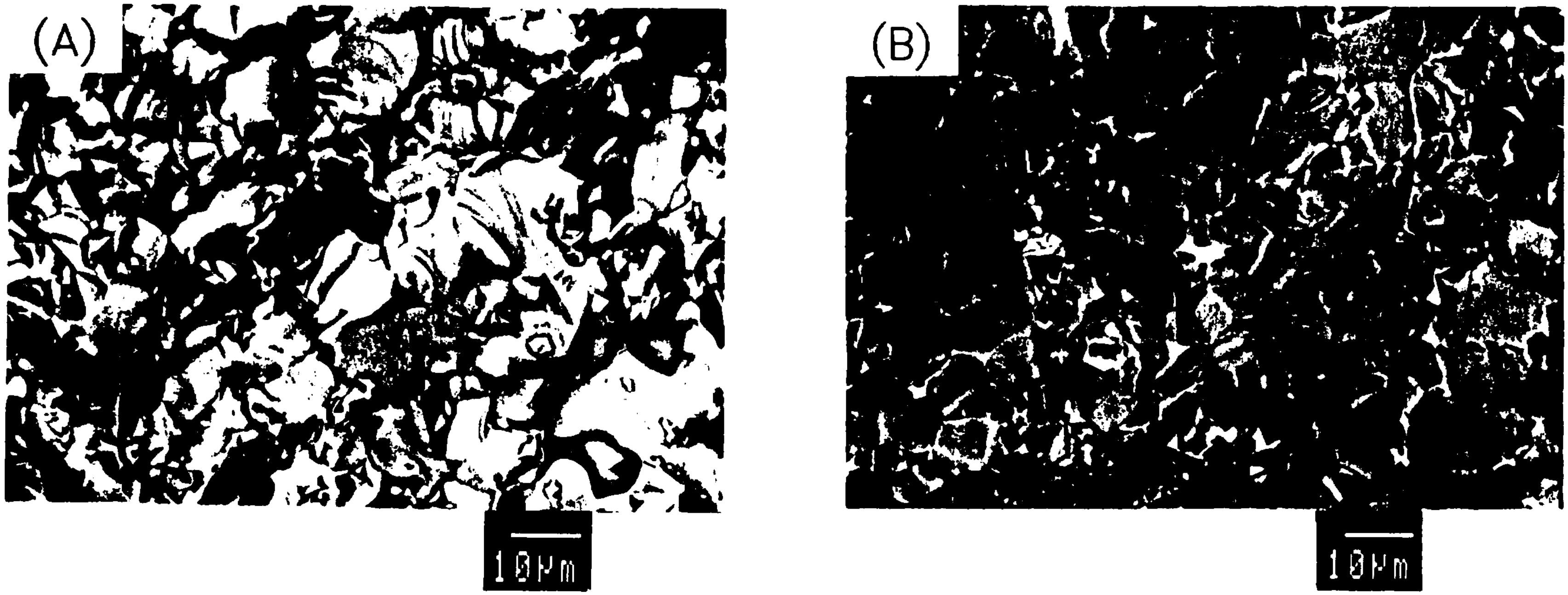

Figure 10. Fractographs of SHS/DC TiC-TiB_2 Composite Structures with a TiB_2/TiC ratio of 0.25. Sample DC11 (Iron-Free) in 10A and Sample DC8 (Iron-Contaminated) in 10B.

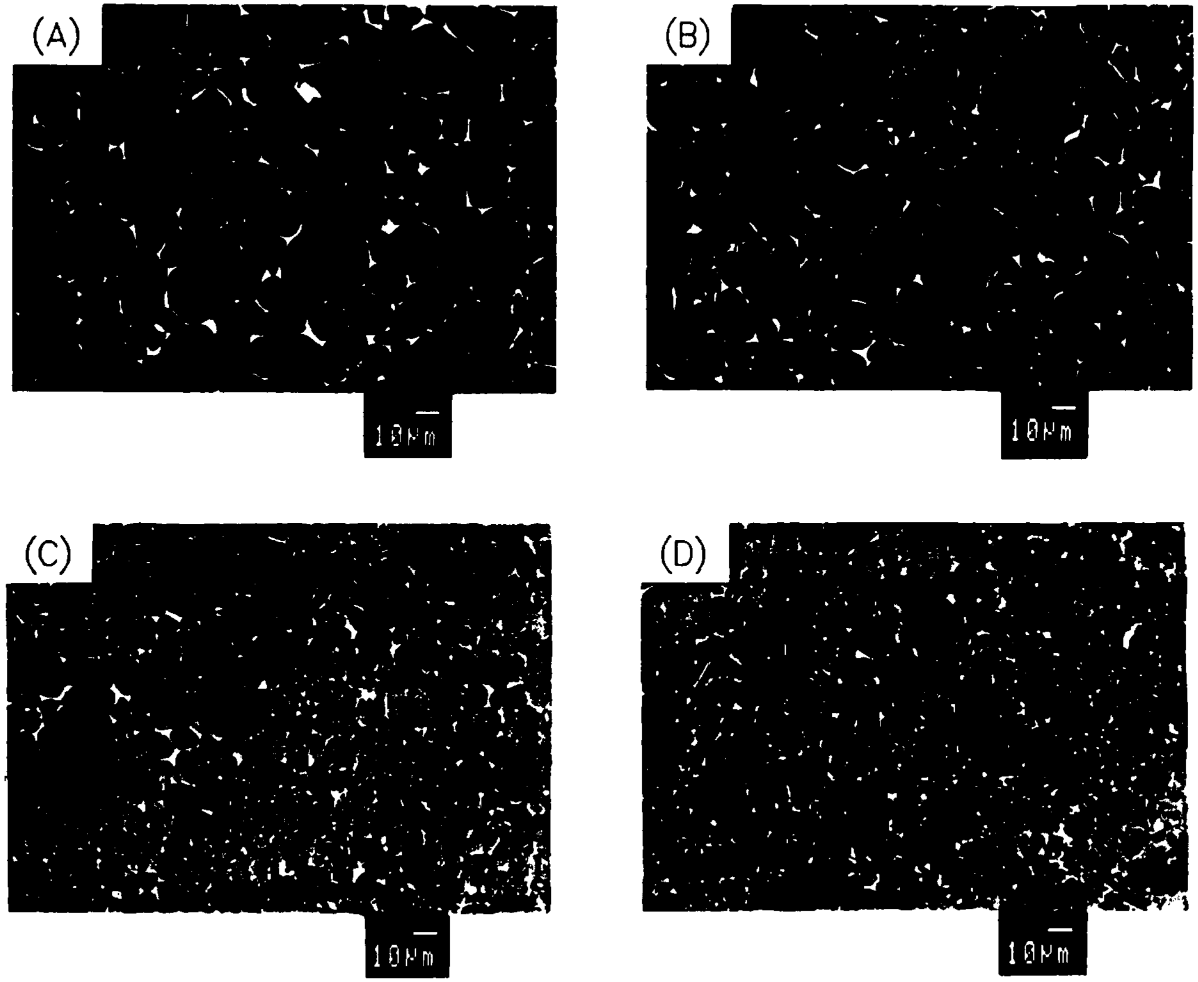

Figure 11. Polished Cross-Sections of SHS/DC TiC-TiB_2 Composite Structures with DC10 (TiC only) Sample in 11A, DC7 (TiB_2/TiC = 0.11) Sample in 11B, DC8 (TiB_2/TiC = 0.25) Sample in 11C, and DC9 (TiB_2/TiC = 0.43) Sample in 11D.

millimeter-sized, closed type of porosity also appears. These larger pores tend to be lenticular, having very large length-to-width aspect ratios, and are usually found in the central regions of the TiC-TiB_2 ceramic disk. The smaller closed porosity is most likely caused by an insufficient consolidation of the porous TiC product. The secondary porosity, however, is probably caused by larger amounts of volatile impurities generated by the TiB_2 reaction. Specifically, during the consolidation event, the molten TiB_2 in the TiC lattice may seal possible exit routes, thereby preventing the trapped gases from escaping.

The fracture properties of the TiC-TiB_2 composites are illustrated in Figure 12 with the DC10 sample in 12A, DC7 sample in 12B, DC8 sample in 12C, and DC9 sample in 12D. The sample fractographs indicate that when there is no TiB_2 present, the fracture mode is nominally transgranular. However, as the amount of TiB_2 in the composite increases, the failure mode becomes increasingly intergranular. As is evident in the fractographs, the addition of TiB_2 reduces the average TiC grain size and appears to arrest grain growth. It is suspected that in the presence of the iron impurity, the decrease in grain size and corresponding increase in surface area cause the average bond strength to decrease, which results in an overall weakness of intergrain bonds in the composite structure (Holleck, Leiste and Schneider 1987, 149-154).

The densities of the TiC-TiB_2 samples are about 93% T.D. and do not indicate an improvement in the ease of densification with increasing amounts of TiB_2 (see Table 4). When compared to the density of DC10, the reduction in the densities of the DC7 and DC8 samples suggests a decrease in compactability of the reaction product. Nonetheless, the decrease in density or, conversely, an increase in sample buoyancy during the density measurement may be attributed to the closed, TiB_2-dependent, macropores of the samples. The microhardnesses of the samples do not appear to improve with the addition of TiB_2 to TiC. Possibly, the TiB_2 crystals are so small and so well dispersed in the TiC matrix that when the indent is made the much harder TiB_2 crystals, without actually deforming, are just pushed into the softer TiC matrix.

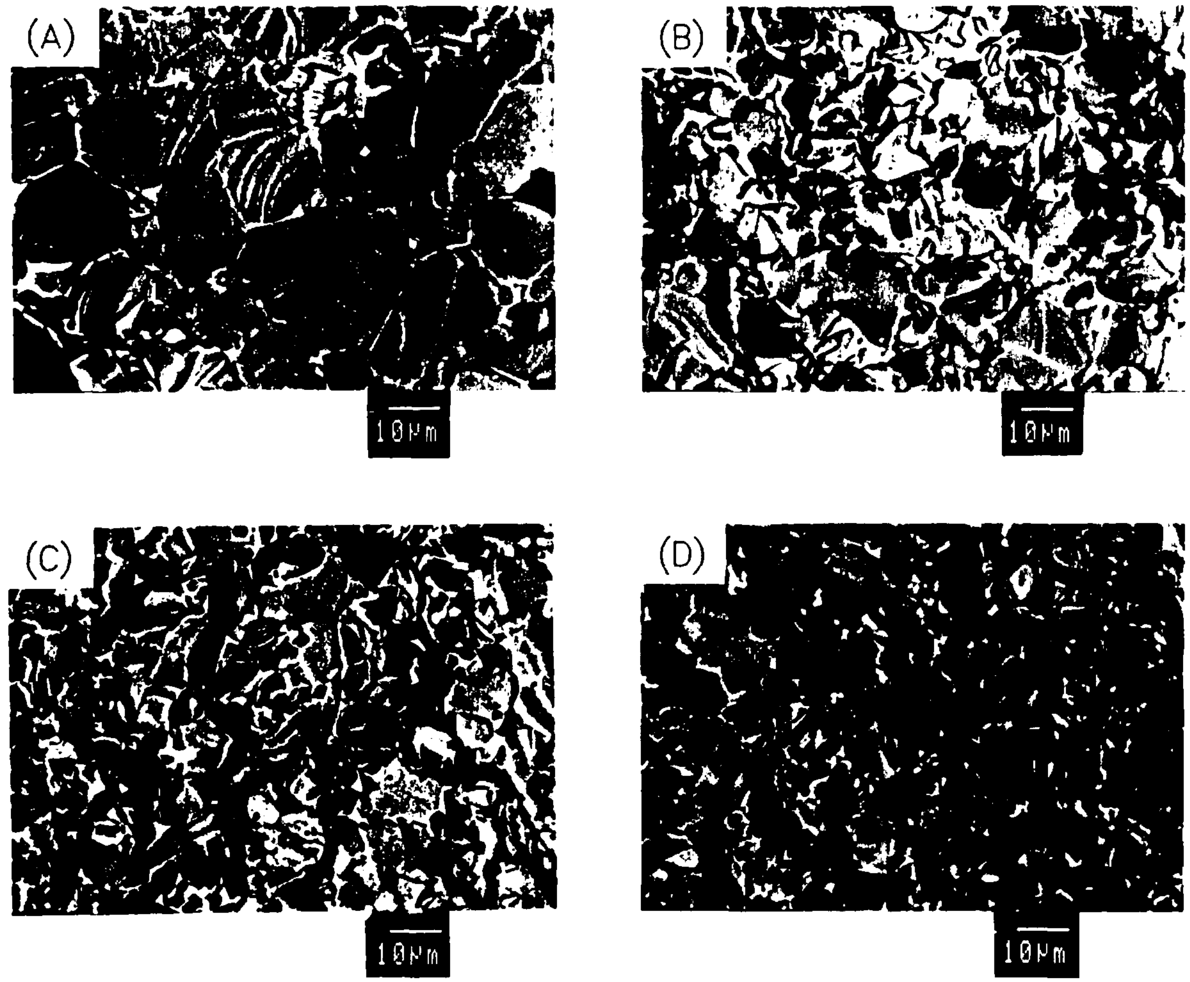

Figure 12. Fractographs of SHS/DC TiC-TiB_2 Composite Structures with DC10 (TiC only) Sample in 12A, DC7 (TiB_2/TiC = 0.11) Sample in 12B, DC8 (TiB_2/TiC = 0.25) Sample in 12C, and DC9 (TiB_2/TiC = 0.43) Sample in 12D.

4. CONCLUSIONS

In this study, SHS/DC TiB_2 and TiC samples have been produced at 98.0% T.D. and microhardness values which are equal to or greater than commercially available hot-pressed materials. Both TiB_2 and TiC possess fracture properties that indicate an improvement in intergrain bonding. The density of SHS/DC TiC with iron-free powders is slightly lower than its hot-pressed equivalent, but its microhardness is comparable or possibly greater.

Several factors which influence the product microstructure of both ceramics have been identified. At the SHS reaction temperatures, most of the solid or "non-volatile" impurities have high enough vapor pressures to volatilize. However, it has been shown that the evolution from the product or the self-purifying nature of the SHS process is limited. If the SHS reaction is carried out with powders containing "non-volatile" contaminants, significant amounts of these impurities will remain in the product, degrading the mechanical integrity. If a metal (e.g., iron) remains in the grain boundaries, it may not only prevent sintering and grain growth but may also weaken intergrain bonding, especially at high temperatures. Furthermore, the presence of a low temperature phase in the grain boundaries limits the use of the ceramic to temperatures below the melting point of such phases. In TiC, the C/Ti ratio significantly alters the structure of the product TiC. The SHS/DC product has maximum density and intrinsic hardness at C/Ti of 1.0. While densification improves with lower C/Ti ratios, such values result in a corresponding drop in sample microhardness. Consequently, the ideal composition for TiC made with the SHS/DC technique may be with a C/Ti ratio of 0.95 to 0.90 where sufficient density is achieved without significantly reducing the microhardness.

In the ternary Ti, C, and B mixtures, only TiC and TiB_2 were formed. This is consistent with the combustion synthesis process where all of the components are consumed by the reaction. Since neither density nor microhardness was found to significantly improve with increasing TiB_2 concentration, it is not clear what advantages, if any, the TiC/TiB_2 composite has over TiC alone. However, since the presence of TiB_2 appears to limit grain growth in TiC, small amounts of TiB_2 could be used to provide such control when needed.

5. REFERENCES

Benck, R. F., L. J. Kecskes, and P. H. Netherwood Jr. "Preparation of HfC by Dynamic Compaction of Combustion Synthesized Material." BRL-MR-3764, U.S. Army Ballistic Research Laboratory, Aberdeen Proving Ground, MD, 1989.

Holleck, H., H. Leiste, and W. Schneider. "Significance of Phase Boundaries in Wear Resistant TiC/TiB_2 Materials." Journal of Refractory Hard Metals, Vol. 6, No. 3, pp. 149-154, 1987.

Kecskes, L. J., and A. Niiler. "Impurities in the Combustion Synthesis of Titanium Carbide." Journal of the American Ceramic Society, Vol. 72, No. 4, pp. 655-661, 1989.

Kingman, P. W. Private communication, U.S. Army Ballistic Research Laboratory, Aberdeen Proving Ground, MD, 12 April 1989.

Kny, E., and H. M. Ortner. "Aspects of Trace Elements in Hard Metals." Proceedings of the International Conference on the Science of Hard Materials, E. A. Almond, C. A. Brookes, and R. Warren, Editors, Adam Higler Ltd., Bristol, England, 1986.

Merzhanov, A. G., I. P. Borovinskaya, L. V. Kustova, and F. I. Dubovitskiy. "Tungsten-Free Hard Alloy and Process for Producing Same." U.S. Patent No. 4,431,448, 1980.

Miracle, D. B., and H. A. Lipsitt. "Mechanical Properties of Fine-Grained Substoichiometric Titanium Carbide." Journal of the American Ceramic Society, Vol. 66, No. 8, pp. 592-597, 1983.

Munir, Z. A. "Synthesis of High Temperature Materials by Self-Propagating Combustion Methods." Ceramic Bulletin, Vol. 67, No. 2, pp. 342-349, 1988.

Niiler, A., L. J. Kecskes, T. Kottke, P. H. Netherwood Jr., and R. F. Benck. "Explosive Consolidation of Combustion Synthesized Ceramics: TiC and TiB_2." BRL-TR-2951, U.S. Army Ballistic Research Laboratory, Aberdeen Proving Ground, MD, 1988.

Niiler, A., L. J. Kecskes, and T. Kottke. "Shock Consolidation of Combustion Synthesized Ceramics." Proceedings of the First International Symposium on Combustion and Plasma-Synthesis of High-Temperature Materials, Z. A. Munir and J. B. Holt, Editors, San Francisco, CA, October 1988.

Niiler, A., L. J. Kecskes, and T. Kottke. "Dynamic Consolidation of Combustion Synthesized TiC and TiB_2." U.S. Army Ballistic Research Laboratory, Aberdeen Proving Ground, MD. To be published.

Ramqvist, L. "Wetting of Metallic Carbides by Liquid Copper, Nickel, Cobalt, and Iron." International Journal of Powder Metallurgy, Vol. 1, No. 4, pp. 2-21, 1965.

Riley, M. A., and A. Niiler. "Low Pressure Compaction of SHS Prepared Ceramics." BRL-MR-3574, U.S. Army Ballistic Research Laboratory, Aberdeen Proving Ground, MD, 1987.

Rudy, E., C. E. Brukl, and D. P. Harmon. "Ternary Phase Equilibria in Transition Metal-Boron-Carbon-Silicon Systems, Part I, Vol II." Air Force Materials Laboratory, AFML-TR-65-2, Wright-Patterson Air Force Base, OH, 1965.

Storms, E. K. Refractory Carbides. Academic Press, New York, NY, 1967.

Toth, L. E. Transition Metal Carbides and Nitrides. Academic Press, New York, NY, 1971.

Yamada, O., Y. Miyamoto, and M. Koizumi. "High Pressure Self-Combustion Sintering of Titanium Carbide." Journal of the American Ceramic Society, Vol. 70, No. 9, pp. c206-c208, 1987.

No of Copies	Organization
1	Office of the Secretary of Defense OUSD(A) Director, Live Fire Testing ATTN: James F. O'Bryon Washington, DC 20301-3110
2	Administrator Defense Technical Info Center ATTN: DTIC-DDA Cameron Station Alexandria, VA 22304-6145
1	HQDA (SARD-TR) WASH DC 20310-0001
1	Commander US Army Materiel Command ATTN: AMCDRA-ST 5001 Eisenhower Avenue Alexandria, VA 22333-0001
1	Commander US Army Laboratory Command ATTN: AMSLC-DL Adelphi, MD 20783-1145
2	Commander US Army, ARDEC ATTN: SMCAR-IMI-I Picatinny Arsenal, NJ 07806-5000
2	Commander US Army, ARDEC ATTN: SMCAR-TDC Picatinny Arsenal, NJ 07806-5000
1	Director Benet Weapons Laboratory US Army, ARDEC ATTN: SMCAR-CCB-TL Watervliet, NY 12189-4050
1	Commander US Army Armament, Munitions and Chemical Command ATTN: SMCAR-ESP-L Rock Island, IL 61299-5000
1	Commander US Army Aviation Systems Command ATTN: AMSAV-DACL 4300 Goodfellow Blvd. St. Louis, MO 63120-1798

No of Copies	Organization
1	Director US Army Aviation Research and Technology Activity ATTN: SAVRT-R (Library) M/S 219-3 Ames Research Center Moffett Field, CA 94035-1000
1	Commander US Army Missile Command ATTN: AMSMI-RD-CS-R (DOC) Redstone Arsenal, AL 35898-5010
1	Commander US Army Tank-Automotive Command ATTN: AMSTA-TSL (Technical Library) Warren, MI 48397-5000
1	Director US Army TRADOC Analysis Command ATTN: ATAA-SL White Sands Missile Range, NM 88002-5502
(Class. only) 1	Commandant US Army Infantry School ATTN: ATSH-CD (Security Mgr.) Fort Benning, GA 31905-5660
(Unclass. only) 1	Commandant US Army Infantry School ATTN: ATSH-CD-CSO-OR Fort Benning, GA 31905-5660
1	Air Force Armament Laboratory ATTN: AFATL/DLODL Eglin AFB, FL 32542-5000

Aberdeen Proving Ground

No of Copies	Organization
2	Dir, USAMSAA ATTN: AMXSY-D AMXSY-MP, H. Cohen
1	Cdr, USATECOM ATTN: AMSTE-TD
3	Cdr, CRDEC, AMCCOM ATTN: SMCCR-RSP-A SMCCR-MU SMCCR-MSI
1	Dir, VLAMO ATTN: AMSLC-VL-D

No. of Copies	Organization
1	Commander US Army Foreign Science and Technical Center ATTN: Mr. J. F. Crider Mr. W. Marley 220 Seventh Street, NE Charlottesville, VA 22901
3	Commander Army Materials Technology Laboratory ATTN: AMXMR-0M Dr. J. V. Marik Dr. W. J. Croft AMXMR-MCP Dr. D. Viechnicki Watertown, MA 02172
3	Commander US Army Research Office ATTN: Dr. I. Ahmad Dr. A. Crowson Dr. R. Reeber P. O. Box 12211 Res Triangle Park, NC 27709
1	National Institute of Science and Technology ATTN: Dr. S. J. Schneider Gaithersburg, MD 20899
2	Director Lawrence Livermore National Laboratory ATTN: Dr. J. B. Holt, L-369 Dr. D. Maiden, MS-L71 P. O. Box 808 Livermore, CA 94550
4	Director Los Alamos National Laboratory ATTN: Dr. R. Behrens, MS-3C348 Dr. K. F. Wylie, MS-G780 Dr. D. Sandstrom, MS-G756 Dr. S. E. Caldwell P. O. Box 1663 Los Alamos, NM 87545

No. of Copies	Organization
1	Director Sandia National Laboratories Applied Mathematics Div 8231 ATTN: Dr. S. B. Margolis Livermore, Ca 94550
3	Idaho Nat. Eng. Laboratory ATTN: Dr. B. H. Rabin Dr. G. E. Korth Dr. R. N. Wright P.O Box 1625 Idaho Falls, ID 83415
1	AIRTRON Division ATTN: Dr. J. Ings 200 East Hanover Ave. Morris Plains, NJ 07950
1	ALCOA Laboratory ALCOA Tech Center ATTN: Dr. A. J. Becker Alcoa Center, PA 15069
1	Battelle Columbus Laboratory ATTN: V. D. Linse Metalworking Section Columbus, OH 43201
1	California Institute of Technology ATTN: Dr. T. D. Vreeland Keck Laboratories, MS138-78 Pasadena, CA 91125
1	Defense Advanced Research Project Agency ATTN: Dr. P. A. Parrish 1400 Wilson Blvd. Arlington, VA 22209
3	General Sciences, Inc. ATTN: Dr. P. D. Zavitsanos Dr. J. J. Gebhardt Mr. M. A. Riley P. O. Box 185 Norristown, PA 10401
2	Georgia Institute of Tech ATTN: Ms. K. V. Logan Dr. J. D. Walton EES/EMSL Atlanta, GA 30332

No. of Copies	Organization
1	Lockheed Palo Alto Research Laboratory ATTN: Dr. A. P. Hardt 3251 Hanover Street Palo Alto, Ca 94304
2	Martin Marietta Laboratories ATTN: Dr. D. C. Nagle Dr. S. R. Winzer 1450 South Rolling Road Baltimore, MD 21227
2	New Mexico Tech ATTN: Dr. N. Thadani Dr. P. A. Persson CETR Socorro, NM 87801
1	New Mexico Tech ATTN: Dr. O. T. Inal Materials/Metallurgical Engr. Socorro, NM 87801
1	Rice University ATTN: Dr. J. Margrave P. O. Box 2692 Houston, TX 77252
3	State University of New York ATTN: Dr. V. Hlavacek Dr. J. Puszynski Dr. S. Majorowski Amherst Campus Furnas Hall 507 Buffalo, NY 14260
1	Terra Tek, Inc. ATTN: R. A. Cutler 400 Wakara Way Salt Lake City, UT 84108
1	University of California ATTN: Dr. Z. Munir College of Engineering Davis, CA 95616

No. of Copies	Organization
1	R. A. Cutler Ceramatec, Inc. 2425 South 900 West Salt Lake City, UT 84119
1	J. W. McCauley NY State College of Ceramics Alfred University Alfred, NY 14802
1	Univ of California, San Diego Dept. of Appl. Mechanics and Engineering Science ATTN: Dr. M. A. Meyers La Jolla, CA 92093
	Alberdeen Proving Ground
	Cdr, CRDEC, AMCCOM ATTN: SMCCR-MUC-T T. R. Racine

No. of Copies	Organization
1	Tokyo Institute of Technology ATTN: Dr. A. Sawaoka Dr. O. Odawara 4259 Nagatsuta Midori-ku Yokohama 227, Japan
1	National Research Institute for Metals ATTN: Kaieda, Yoshinari 2-3-12 Nakameguro, Meguro-ku Tokyo 153, Japan
1	Ryukoku University ATTN: Koizumi, Mitsue 1-5 Yokoya, Oe-cho, Seta, Otsu Shiga 520-21, Japan
1	Osaka University ATTN: Miyamoto, Yoshinari Ibaraki, Osaka 567, Japan
1	Government Industrial Research Institute, Tohoku ATTN: Sata, Nobuhiro 4-5-1 Nigatake, Miyagino-ku, Sendai Miyagi 983, Japan

USER EVALUATION SHEET/CHANGE OF ADDRESS

This Laboratory undertakes a continuing effort to improve the quality of the reports it publishes. Your comments/answers to the items/questions below will aid us in our efforts.

1. BRL Report Number BRL-TR-3133 Date of Report AUGUST 1990

2. Date Report Received ____________________

3. Does this report satisfy a need? (Comment on purpose, related project, or other area of interest for which the report will be used.) ____________________

4. Specifically, how is the report being used? (Information source, design data, procedure, source of ideas, etc.) ____________________

5. Has the information in this report led to any quantitative savings as far as man-hours or dollars saved, operating costs avoided, or efficiencies achieved, etc? If so, please elaborate. ____________________

6. General Comments. What do you think should be changed to improve future reports? (Indicate changes to organization, technical content, format, etc.) ____________________

CURRENT ADDRESS

Name

Organization

Address

City, State, Zip Code

7. If indicating a Change of Address or Address Correction, please provide the New or Correct Address in Block 6 above and the Old or Incorrect address below.

OLD ADDRESS

Name

Organization

Address

City, State, Zip Code

(Remove this sheet, fold as indicated, staple or tape closed, and mail.)

--------------------FOLD HERE--------------------

DEPARTMENT OF THE ARMY

Director
U.S. Army Ballistic Research Laboratory
ATTN: SLCBR-DD-T
Aberdeen Proving Ground, MD 2100[illegible]-5066

OFFICIAL BUSINESS

NO POSTAGE NECESSARY IF MAILED IN THE UNITED STATES

BUSINESS REPLY MAIL
FIRST CLASS PERMIT No 0001, APG, MD

POSTAGE WILL BE PAID BY ADDRESSEE

Director
U.S. Army Ballistic Research Laboratory
ATTN: SLCBR-DD-T
Aberdeen Proving Ground, MD 21005-9989

--------------------FOLD HERE--------------------